Macromolecules

Article

pubs.acs.org/Macromolecules

Whispering Gallery Resonance from Self-Assembled Microspheres of Highly Fluorescent Isolated Conjugated Polymers

Soh Kushida,[†] Daniel Braam,[‡] Chengjun Pan,[§] Thang D. Dao,[∥,⊥,#] Kenichi Tabata,[†] Kazunori Sugiyasu,[§] Masayuki Takeuchi,[§] Satoshi Ishii,[∥,⊥] Tadaaki Nagao,[∥,⊥] Axel Lorke,[‡] and Yohei Yamamoto*[,†]

[†]Division of Materials Science and Tsukuba Research Center for Interdisciplinary Materials Science (TIMS), Faculty of Pure and Applied Sciences, University of Tsukuba, 1-1-1 Tennodai, Tsukuba, Ibaraki 305-8573, Japan

[‡]Faculty of Physics and CENIDE, University of Duisburg-Essen, Lotharstraβe 1, Duisburg D-47048, Germany

[§]Organic Materials Group, Polymer Material Unit, National Institute for Materials Science, 1-2-1 Sengen, Tsukuba, Ibaraki 305-0047, Japan

[∥]International Center for Materials Nanoarchitectonics (MANA), National Institute for Materials Science (NIMS), 1-1 Namiki, Tsukuba, Ibaraki 305-0044, Japan

[⊥]CREST, Japan Science and Technology Agency, 4-1-8 Honcho, Kawaguchi, Saitama 332-0012, Japan

[#]Graduate School of Materials Science, Nara Institute of Science and Technology, 8916-5 Takayama, Ikoma, Nara 630-0192, Japan

Supporting Information

ABSTRACT: Self-assembly of highly fluorescent isolated conjugated polymers (ICPs), comprising alternating phenylene moieties with an insulating cyclic side chain and different arylene moieties, was comprehensively studied. Two out of nine ICPs were identified to form well-defined spheres of 1−6 μm diameter. The degree of twisting of the main chains was found to be an important structural factor enabling formation of spheres, for which dihedral angles >50° between the neighboring arylene moieties were required. A single microsphere with high sphericity exhibited whispering gallery mode (WGM) photoemission upon excitation with a focused laser. In this emission, sharp and periodic emission lines were superimposed on a broad photoemission spectrum. The WGM spectral profiles were very sensitive to the integrity of the spherical geometries and surface smoothness, which depends on the self-assembling condition as well as the structure of the polymer backbone. Microspherical optical resonators consisting of such highly fluorescent conjugated polymers are novel. They also present advantages in that (i) there is no need for a light waveguide and fluorescent-dye doping, (ii) its high refractive index is beneficial for light confinement, and (iii) the fabrication process is simple, not requiring sophisticated, costly microfabrication technology.

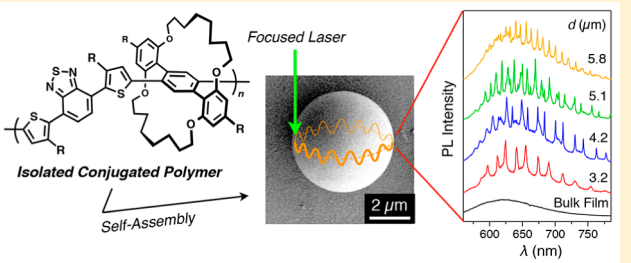

INTRODUCTION

π-Conjugated polymers possess charge transport, photoemission, and redox properties, which are useful for applications in electronic and optoelectronic devices such as light-emitting diodes, transistors, solar cells, and electrochromic devices.[1−6] Recently, spherical colloids formed from π-conjugated polymers have attracted attention for additional optical and biomedical applications involving fluorescence imaging, drug and gene delivery, and colloidal photonic crystals.[7−9] However, in general, π-conjugated polymers are hard to form into well-defined spheres because of their rigid and planar backbones. Thus, there have been few examples of π-conjugated polymer spheres reported so far.[8,10−16] Moreover, most of these were prepared using miniemulsion polymerization and dispersion polymerization methods.

In this context, we have recently reported several π-conjugated alternating copolymers that form well-defined microspheres quantitatively via self-assembly in a thermodynamic solution process.[17,18] The slow diffusion of a polar nonsolvent vapor into a solution of a low-crystallinity polymer results in the formation of spheres with diameters in the submicrometer to several micrometers range. Interestingly, upon laser excitation of a single sphere, clear whispering gallery modes (WGM) were observed in photoemission.[19] Because the refractive indices (η) of these polymers are in the range of 1.6−1.8, which is high enough in comparison with the refractive index of air ($\eta_{air} \sim 1.0$), fluorescence generated inside the microspheres is efficiently confined via total internal reflection at the polymer/air interface. As a result, sharp and periodic emission lines appear in their photoluminescence spectra with Q-factors up to 600. Fabry−Perot cavities have been realized from single crystals of low-molecular-weight organic molecules and used to generate laser action in entirely organic, solid materials.[3,20−24] Here, the laser cavity was formed using the

Received: April 6, 2015
Revised: June 5, 2015

DOI: 10.1021/acs.macromol.5b00707
Macromolecules XXXX, XXX, XXX−XXX

opposing single-crystal facets as mirrors. On the other hand, for noncrystalline materials such as polymers, microspherical and microring resonators are a more promising route to high finesse optical cavities.[25−31] However, one drawback of the fluorescent microresonators we reported is attributed to the low intrinsic photoemission properties of the copolymers, which exhibit an absolute fluorescent quantum yield (ϕ_{FL}) of less than 0.02 in their solid state.[19,32,33]

In this article, we focus our attention on isolated conjugated polymers (ICPs).[34−40] Most ICPs show high ϕ_{FL} even in the solid state because their π-conjugated main chains are highly isolated from one another by insulating cyclic side chains. This leads to effective suppression of nonradiative decay from their excited state. Another advantage is that the ICPs possess low crystallinity, resulting in the formation of amorphous films when they are drop-cast from solution.[38] Low crystallinity is a key factor enabling formation of spheres through self-assembly.[17,18] We attempted self-assembly of nine ICPs (Figure 1) through a vapor diffusion process in solution and found that

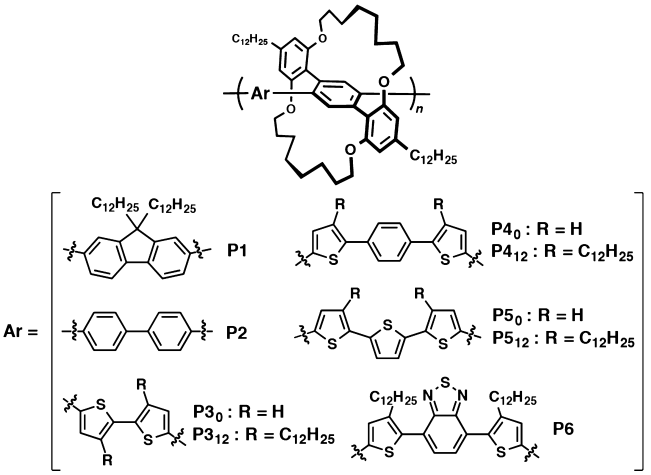

Figure 1. Molecular structures of isolated conjugated polymers (ICPs) **P1**−**P6**.

two of these formed well-defined microspheres. Furthermore, the photoemission spectra of isolated single microspheres formed from one ICP (ϕ_{FL} = 0.13) exhibited WGM photoemission with *Q*-factors up to ∼900. The WGM resonance spectral profiles quite sensitively detected the degree of integrity of the sphere morphology and surface roughness.

MATERIALS AND METHODS

Synthesis and Self-Assembly of Isolated Conjugated Polymers. In this study, we prepared ICPs **P1**−**P6**, which are all alternating copolymers containing a phenylene moiety covered with 1,10,17,26-tetraoxa[10.10]metacyclophane as one part and arylene (Ar) groups such as 9,9-di-*n*-dodecylfluorene (**P1**), biphenylene (**P2**), 2,2′-bithiophene (**P3$_0$**), 3,3′-di-*n*-dodecyl-2,2′-bithiophene (**P3$_{12}$**), thiophene−phenylene−thiophene (**P4$_0$**), 3-*n*-dodecylthiophene−phenylene−3′-*n*-dodecylthiophene (**P4$_{12}$**), 2,2′:5′,2″-terthiophene (**P5$_0$**), 3′,3″-di-*n*-dodecyl-2,2′:5′,2″-terthiophene (**P5$_{12}$**), and 3-*n*-dodecylthiophene−benzothiadiazole−3′-*n*-dodecylthiophene (**P6**) as the counterpart (Figure 1). Procedures for the synthesis of these copolymers are described in the Supporting Information (**P2**, **P3$_0$**, **P4$_0$**, **P4$_{12}$**, and **P5$_0$**) and references (**P1**, **P3$_{12}$**, **P5$_{12}$**, and **P6**).[38,40] The number-average molecular weight (M_n) and polydispersity index (PDI) of the copolymers are described in Table 1, along with their photoabsorption and emission properties in the film state.[38] The wavelengths of the

Table 1. Number-Average Molecular Weight (M_n), Polydispersity Index (PDI), Wavelength of Maximum Absorption (λ_{abs}) and Emission (λ_{em}), Fluorescence Quantum Yield (ϕ_{FL}) in the Solid State, and Morphology of the Self-Assembled Precipitates of P1−P6

	M_n/kg mol^{-1} (PDI[a])	λ_{abs}/nm	λ_{em}/nm	ϕ_{FL}	morphology[b]
P1[c]	10.6 (1.3)	338	398	0.44	×
P2	10.4 (1.5)	325	395	0.49	×
P3$_0$	20.0 (1.9)	439	511	0.076	×
P3$_{12}$[c]	22.6 (2.9)	381	482	0.12	◎
P4$_0$	7.5 (1.3)	422	491	0.28	△
P4$_{12}$	11.4 (1.8)	390	479	0.31	△
P5$_0$	22.0 (1.8)	463	550	0.090	△
P5$_{12}$[c]	21.2 (1.8)	443	539	0.18	△/×
P6[c]	8.4 (1.2)	481	631	0.13	◎

[a]Weight-average molecular weight (M_w) divided by M_n. [b]◎, well-defined spheres; △, distorted or rough spheres; ×, irregular aggregates or nanofibers. [c]Reference 38.

emission maxima are in the range 395−631 nm, and the ϕ_{FL} in the solid state are in the range 0.076−0.49.

Self-assembly of the copolymers was carried out using the vapor diffusion method (Figure S1).[17,18] Typically, a 5 mL vial containing 2 mL of $CHCl_3$ or CH_2Cl_2 solution of the copolymers (0.5 mg mL^{-1}) was placed in a 50 mL vial containing 5 mL of a nonsolvent such as MeOH, acetonitrile (MeCN), acetone, or hexane. The outside vial was capped and then kept for 3 days at 25 °C, resulting in a suspension of self-assembled precipitates.

Microphotoluminescence (μ-PL) Measurements. Measurements of μ-PL were carried out using a μ-PL measurement system (Figure S2).[41] An optical microscope was used with a long-distance 50× or 100× objective (NA = 0.5 or 0.8) to identify suitable particles and to determine their diameters (d). For excitation at λ = 405 nm, a Linos model Nano 250 continuous wave diode laser was used with the power, integration time, and spot size of 1.0 μW, 0.1 s, and ∼0.5 μm, respectively. PL was detected using a 0.5 m Czerny Turner spectrometer (Acton model SpectraPro 2500i with 0.26 nm resolution) with a LN_2-cooled charge-coupled device (CCD) detector. For excitation at λ = 532 nm, a WITec μ-PL system was used with a model Alpha 300S microscope combined with a Princeton Instruments model Action SP2300 monochromator (grating: 300 grooves mm^{-1}) and an Andor iDus model DU-401A BR-DD-352 CCD camera cooled to −60 °C. A continuous wave diode-pumped solid state (second harmonic generator) laser (S/N: 100−1665−132) was used with the power, integration time, and spot size of 1.5 μW, 0.5 s, and ∼0.5 μm, respectively. The self-assembled microspheres were mounted on a quartz substrate by spin-casting the suspension of the spheres. The edge part of a single sphere was excited by continuous-wave laser light at 25 °C under ambient condition.

RESULTS AND DISCUSSION

Self-Assembly of Isolated Conjugated Polymers. Figure 2 displays scanning electron microscopy (SEM) images of the precipitates resulting from the representative solvent combinations (for other combinations, see Figures S3−S11 and Tables S1−S9). Irregular and nanofibrous aggregates resulted from self-assembly of **P1**, **P2**, and **P3$_0$** (Figure 2a−c, respectively). Particles of **P4$_0$**, **P4$_{12}$**, **P5$_0$**, and **P5$_{12}$** were nearly spherical under several assembly conditions, but their surfaces were very rough or wrinkled (Figure 2e−h). In contrast, self-assembly of **P3$_{12}$** (Figure 2d) and **P6** (Figure 2i and j) produced well-defined spherical microstructures using several solvent combinations. For example, for the self-assembly of **P6**, CH_2Cl_2 and MeCN as solvent and nonsolvent, respectively, resulted in spheres with d of 2−6 μm (Figure 2i), while the

DOI: 10.1021/acs.macromol.5b00707
Macromolecules XXXX, XXX, XXX−XXX

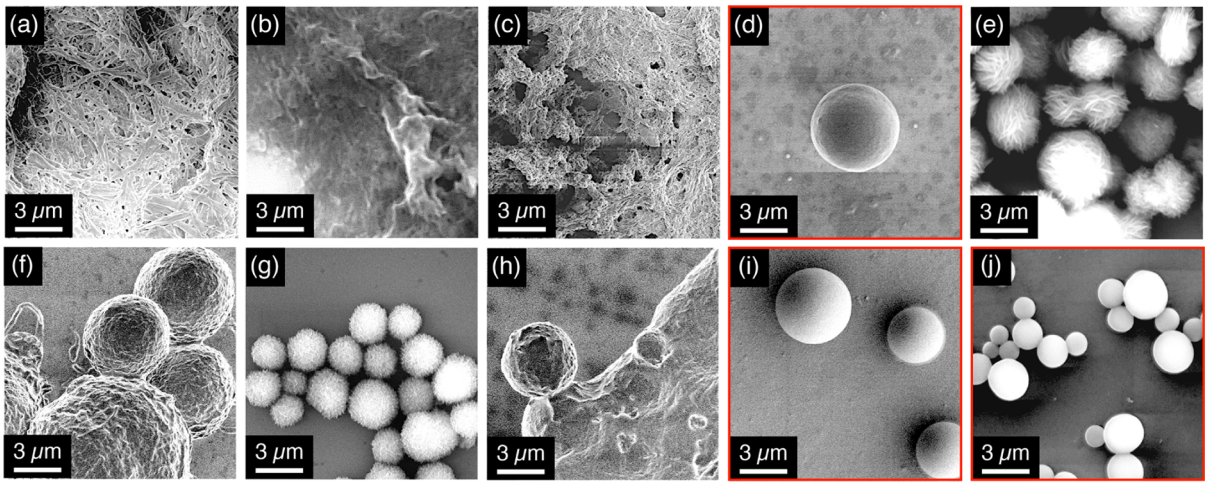

Figure 2. SEM micrographs of air-dried suspensions of **P1** (a), **P2** (b), $\mathbf{P3_0}$ (c), $\mathbf{P3_{12}}$ (d), $\mathbf{P4_0}$ (e), $\mathbf{P4_{12}}$ (f), $\mathbf{P5_0}$ (g), $\mathbf{P5_{12}}$ (h), and **P6** (i, j) self-assembled with the solvent−nonsolvent combinations $CHCl_3$−MeOH (b, d, h), $CHCl_3$−MeCN (a, c, e, f, j), $CHCl_3$−acetone (g), and CH_2Cl_2−MeCN (i). The images in the red squares (d, i, j) indicate that well-defined microspheres form in the precipitates.

Table 2. Expected Molecular Configurations and Dihedral Angles of the Ar Moieties in P2−P6 with and without Methyl Groups (Left: Top View; Right: Side View) by B3LYP/6-31G* Level DFT Calculations[a]

	P2	$\mathbf{P3_0}$, $\mathbf{P3_{12}}$	$\mathbf{P4_0}$, $\mathbf{P4_{12}}$	$\mathbf{P5_0}$, $\mathbf{P5_{12}}$	**P6**
w/o Me Groups	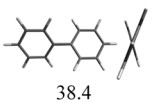	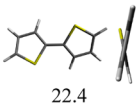	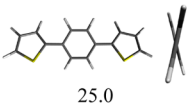	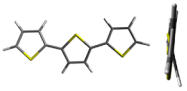	–
Dihedral Angle (°)	38.4	22.4	25.0	19.2	
with Me Groups	–	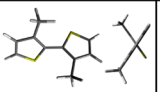	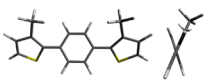	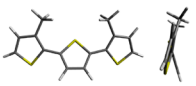	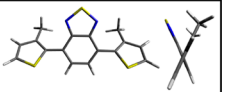
Dihedral Angle (°)		65.4	42.8	29.0	50.0

[a]Molecular models: biphenyl for **P2**, 2,2′-bithiophene for $\mathbf{P3_0}$, 3,3′-dimethyl-2,2′-bithiophene for $\mathbf{P3_{12}}$, thiophene−phenylene−thiophene for $\mathbf{P4_0}$, 3-methylthiophene−phenylene−3′-methylthiophene for $\mathbf{P4_{12}}$, 2,2′:5′,2″-terthiophene for $\mathbf{P5_0}$, 3,3″-dimethyl-2,2′:5′,2″-terthiophene for $\mathbf{P5_{12}}$, and 3-methylthiophene−benzothiadiazole−3′-methylthiophene for **P6**.

combination of $CHCl_3$ and MeCN resulted in smaller spheres (d of 1−4.5 μm, Figure 2j).

We previously reported that alternating copolymers containing a 3,3′,4,4′-tetramethyl-2,2′-bithiophene unit as one of the structural components effectively produced well-defined spherical assemblies.[18] The steric hindrance between the methyl groups at the 3- and 3′-positions, a so-called head-to-head linkage, induces a highly twisted main chain with a dihedral angle of ∼66° between the neighboring thiophene rings. The severe twisting of the main chain is thought to inhibit interchain π-stacking, leading to an amorphous aggregation of the copolymers into geometrically isotropic spheres. For the ICPs in the present study, the cyclic side chains should prevent the interchain π-stacking; however, only $\mathbf{P3_{12}}$ and **P6** were observed to form well-defined microspheres. In the case of $\mathbf{P3_{12}}$, dodecyl side chains are attached with a head-to-head configuration, resulting in a large steric hindrance and leading to severe twisting of the main chain. The benzothiadiazole moiety in **P6** also works as a large steric hindrance with the neighboring alkyl chains on the thiophene moieties. On the other hand, in the case of $\mathbf{P3_0}$, $\mathbf{P4_0}$, $\mathbf{P4_{12}}$, $\mathbf{P5_0}$, and $\mathbf{P5_{12}}$, head-to-head linkage was absent along the backbone (Figure 1). This meant that the twisting of the main chain was insignificant, resulting in ill-defined microspheres. More rigid and linear **P1** and **P2** formed anisotropic aggregates, i.e., nanofibrous assemblies.

In fact, the density functional theory (DFT) calculations of representative molecular models reveal that a dihedral angle between two thiophene rings in $\mathbf{P3_{12}}$ is 65.4° and that between thiophene and benzothiadiazole rings in **P6** is 50.0°. These are certainly larger than those between neighboring rings in **P2**, $\mathbf{P3_0}$, $\mathbf{P4_0}$, $\mathbf{P4_{12}}$, $\mathbf{P5_0}$, and $\mathbf{P5_{12}}$ (19°−43°, Table 2). Therefore, it is likely that the twisting of the neighboring Ar moiety with dihedral angle of more than 50° is important not only to prevent interchain π-stacking but also to dictate the random coil conformation of the main chain.[42] These two factors determine whether polymers form well-defined microspheres or not.

We reported that π-conjugated polymers with higher number-average molecular weight (M_n) tend to form smaller spheres due to their lower solubility and much more rapid precipitation in comparison with polymers of identical molecular backbones but smaller M_n.[17] In the present study, details of M_n dependency on the size of the resultant microspheres have not been investigated, but a similar tendency should be expected for ICPs. We also expect that the polydispersity index (PDI) affects the nucleation process of the polymer assembly, in which higher PDI possibly results in a much larger size distribution of the size of the spheres.[17]

DOI: 10.1021/acs.macromol.5b00707
Macromolecules XXXX, XXX, XXX−XXX

Whispering Gallery Mode Photoemission from Microspheres of Isolated Conjugated Polymers. Microphotoluminescence (μ-PL) measurements[41] were conducted on the well-defined microspheres formed from **P6**. The microspheres of **P6** prepared from the solvent−nonsolvent combination CH_2Cl_2−MeCN (Figure 2i) exhibited sharp and periodic photoemission lines, superimposed upon the broad photoemission spectrum (Figure 3a). The interval between the

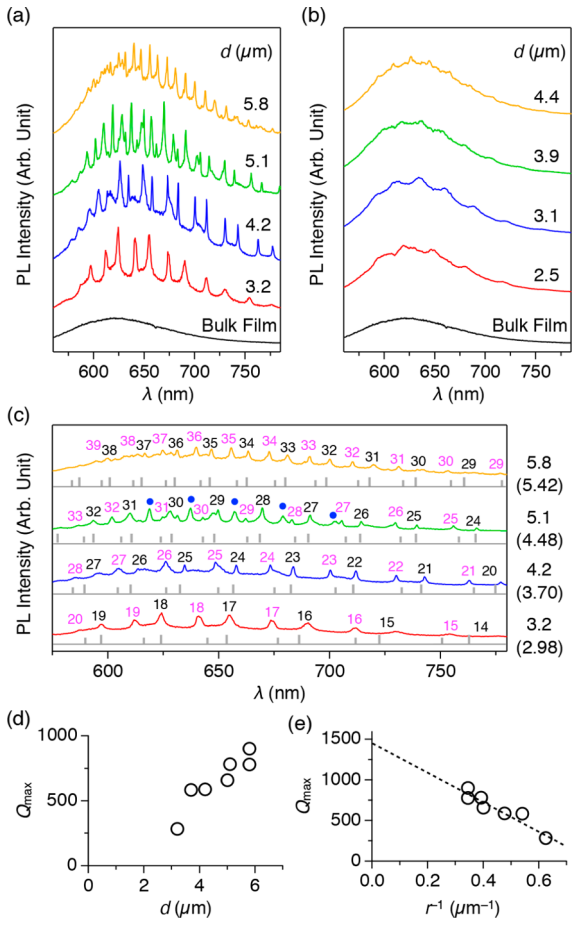

Figure 3. (a, b) Photoluminescence (PL) spectra of different single spheres and a film cast from solution (bulk film) of **P6** upon laser excitation (λ_{ex} = 405 or 532 nm) with a spot size of ~0.5 μm. The spheres were prepared by self-assembly with solvent−nonsolvent combinations CH_2Cl_2−MeCN (a) and $CHCl_3$−MeCN (b). The values indicate d of the spheres, estimated by OM. (c) Simulated emission lines (gray), using eqs 1 and 2, along with the corresponding spectra in (a) . The numbers in black and pink indicate the n-th TE and TM WGM, respectively. The blue dots in the spectrum of the d = 5.1 μm sphere indicate the higher order WGMs. The values and those in parentheses indicate d estimated by OM and by the simulation, respectively. (d, e) Plots of Q_{max} (circles) versus d and reciprocal radius (r^{-1}) of the microspheres of **P6**. The dotted line in (e) indicates the extrapolation of the least-squares fit to the phenomenological equation; $Q_{max} = -1777r^{-1} + 1447$.

emission lines became smaller as d of the spheres increased from 3.2 to 5.8 μm. In contrast, such sharp emission lines were never observed from a cast film of **P6** prepared from $CHCl_3$ solution (Figure 3a, black).

The observed periodic photoemission peaks were identified as WGM photoemission,[19,25−31] where the fluorescence generated inside the sphere was confined via total internal reflection at the polymer/air interface and which self-interferes after traveling the circumference of the sphere. The fitting simulations of the WGM emission lines were conducted using eqs 1 and 2 for transverse electric (TE) and magnetic (TM) mode emissions, respectively[27]

$$\lambda_n^E = 2\pi r(\varepsilon\mu)^{1/2}\left[\left(n+\frac{1}{2}\right) + 1.85576\left(n+\frac{1}{2}\right)^{1/3} - \frac{1}{\varepsilon}\left(\frac{\varepsilon\mu}{\varepsilon\mu-1}\right)^{1/2}\right]^{-1} \quad (1)$$

$$\lambda_n^H = 2\pi r(\varepsilon\mu)^{1/2}\left[\left(n+\frac{1}{2}\right) + 1.85576\left(n+\frac{1}{2}\right)^{1/3} - \frac{1}{\mu}\left(\frac{\varepsilon\mu}{\varepsilon\mu-1}\right)^{1/2}\right]^{-1} \quad (2)$$

where λ_n^E and λ_n^H are the wavelengths of the nth TE and TM mode photoemission, respectively, ε (= η^2) is the dielectric permittivity, μ (= 1) is the magnetic permeability, and r is the sphere's radius. Here, the much higher-order term was neglected. The average η values for **P6** (~1.60) was obtained by spectroscopic ellipsometry measurements (Figure S12). The positions of the observed emission lines corresponded well with those of the simulated lines with TE and TM modes (Figure 3c). The sphere with d = 5.1 μm displayed very complicated emission lines with higher order TE and TM modes, in addition to the first-order TE and TM modes.[31] The d values evaluated by the fitting simulation, denoted in parentheses in Figure 3c, are smaller than those observed by optical microscopy (OM). Within the margin of error of the sphere's radius given by OM, the simulation adapts the radius so that both TE and TM modes agree well for given orders n, effectively determining the radius with much higher precision. We also attempted peak fitting using wavelength-dependent η values obtained from ellipsometry data. However, the simulated peak positions and obtained diameters were much deviated from the corresponding spectra in comparison with that using the average η value (Figure S13).

The Q-factors, approximated by the peak wavelength divided by the full width at half-maximum of the peak, increased as d of the sphere increased and the maximum value reached 900 for the spheres with d = 5.8 μm (Figure 3d and Table S10). This value (Q_{max}) was 1.5-fold higher than that previously reported for the π-conjugated polymer microsphere with much larger d (Q_{max} ~ 600 for d = 10 μm sphere).[19] One possible reason for such high Q-factors is lower attenuation of the present microspheres. According to the ellipsometry study (Figure S12), the k value at the photoemission wavelength range of **P6** was less than 0.08, which is smaller than those of the previously reported polymers (k ~ 0.2).[19] The plots of Q_{max} versus reciprocal radius, i.e., the curvature of the spheres, showed an approximately linear correlation (Figure 3e) because the bending radiation loss of circular resonators declines as the curvature decreases.[19,43] In addition, we checked the excitation power dependency of the PL spectra and the intensity of WGM emission peaks (Figure S14). The double-logarithmic plot shows that the PL intensity increased linearly in the power range of 1−100 μW. Upon further increase of the pump power to 1000 μW, the WGM peak weakened, and the slope of the peak intensity plot was suppressed to some extent. This behavior indicates that the sphere was damaged upon pumping with the CW laser, before exceeding the laser oscillation threshold.

In contrast, microspheres of **P6** prepared from another solvent−nonsolvent combination ($CHCl_3$−MeCN, Figure 2j)

DOI: 10.1021/acs.macromol.5b00707
Macromolecules XXXX, XXX, XXX−XXX

did not show such sharp photoemission lines, but only a weak intensity modulation (Figure 3b). The objects self-assembled from this condition were superficially regarded as well-defined spheres (Figure 2j). However, closer analysis of their morphology indicated that these particles were distorted to some extent, and their shapes deviated from the exact spheres.

Figures 4a and 4b show magnified SEM images of the self-assembled spheres from **P6**, prepared from solvent−nonsolvent combinations CH_2Cl_2−MeCN (a) and $CHCl_3$−MeCN (b). The pink and green circles indicate inscribed and circumscribed circles with radius r_1 and r_2, respectively. (c) Plots of Δ versus d of the microspheres of **P6** prepared by solvent−nonsolvent combinations CH_2Cl_2−MeCN (red circles) and $CHCl_3$−MeCN (blue triangles). The dotted lines indicate the average Δ for the spheres prepared by each solvent combination.

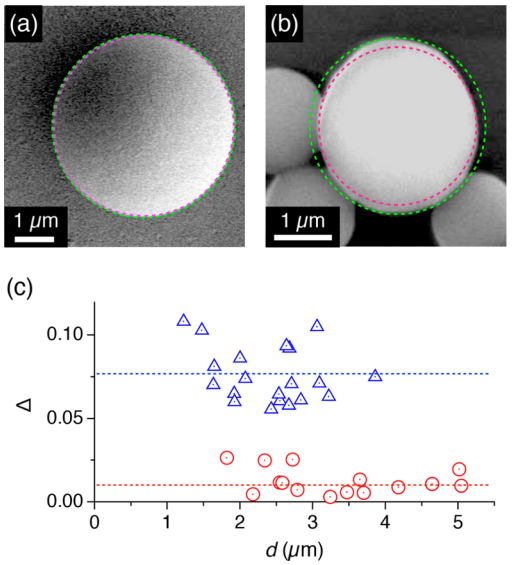

combinations CH_2Cl_2−MeCN and $CHCl_3$−MeCN, respectively, with inscribed (pink, dashed) and circumscribed circles (green, dashed) of radius r_1 and r_2, respectively. We quantified the exactness of the spherical shapes by the relative deviation $\Delta = (r_2 - r_1)/r_2$. The spheres in Figure 3a show an average Δ of 0.012 (Figure 4c, red circles). On the other hand, the average Δ for spheres in Figure 4b was a significantly larger value (0.076, Figure 4c, blue). Note that the Δ values mainly depend on the self-assembly condition and not on the size of the spheres. We estimate that the distortion of the spherical shape in the nucleation and growth process of the polymers results in the surface corrugations. These cause scattering of light at the outer boundary very effectively and suppress the WGM by diffuse reflection and leaking of light out of the sphere.

For comparison, the μ-PL measurements of well-defined microspheres of $\mathbf{P3_{12}}$ were also carried out. However, WGM photoemission lines were hardly observed (Figure S15). This is possibly because the surface of the spheres was not so smooth and the reflection inside the spheres was diffused at the polymer/air interface such that total internal reflection was sufficiently suppressed.

CONCLUSIONS

We investigated the self-assembly of isolated conjugated copolymers with highly fluorescent properties in the solid state and found that two copolymers out of nine formed well-defined microspheres. The relationship between the polymer structure and self-assembled morphology was clearly shown, suggesting that a highly twisted polymer backbone (>50°) is essential for the formation of spherical morphology. Upon laser excitation of a single sphere, clear whispering gallery mode (WGM) photoemission was observed, involving sharp and periodic emission lines in the photoluminescence spectra. The photoemission spectral profiles are quite sensitive to the integrity of the spherical geometry, which is highly dependent on differences in the self-assembly conditions as well as in the structure of the polymer backbone. The similarity of the microparticles to an exact sphere, approximated by their relative range of radii Δ, is an important parameter for achieving WGM resonance. Spheres with $\Delta \sim 0.012$ exhibit pronounced WGM emission lines with maximum Q-factor up to 900. Microspherical optical resonators consisting of such highly fluorescent conjugated polymers are advantageous from the following scientific and technological viewpoints: (i) Conjugated polymers fluoresce directly; therefore, neither light waveguides nor fluorescent dye doping is needed. (ii) Conjugated polymers possess rather high refractive indices; hence, light confinement inside spheres is much more effective than in nonconjugated polymer spheres. (iii) This simple preparation process can be adopted without sophisticated and costly microfabrication technologies.

ASSOCIATED CONTENT

Supporting Information

Materials and measurements, synthesis, MALDI-TOF mass spectrometry, NMR, SEM, ellipsometry, and μ-PL measurements. The Supporting Information is available free of charge on the ACS Publications website at DOI: 10.1021/acs.macromol.5b00707.

AUTHOR INFORMATION

Corresponding Author

*E-mail yamamoto@ims.tsukuba.ac.jp (Y.Y.).

Notes

The authors declare no competing financial interest.

ACKNOWLEDGMENTS

This work was partly supported by a Grant-in-Aid for Young Scientists A (25708020) and Scientific Research on Innovative Areas (No. 26102009, 15H00860, 15H00986) from JSPS/MEXT Japan, SCOPE ICT for young researchers from MIC Japan, Cooperative Research Program of "Network Joint Research Centre for Materials and Devices", Asahi Glass Foundation, Tokuyama Science Foundation, and University of Tsukuba-DAAD partnership program.

REFERENCES

(1) Friend, R. H.; Gymer, R. W.; Holmes, A. B.; Burroughes, J. H.; Marks, R. N.; Taliani, C.; Bradley, D. D. C.; Dos Santos, D. A.; Brédas, J. L.; Lögdlund, M.; Salaneck, W. R. *Nature* **1999**, *397*, 121−128.

(2) Zaumseil, J.; Friend, R. H.; Sirringhaus, H. *Nat. Mater.* **2006**, *5*, 69−74.

(3) Samuel, I. D. W.; Turnbull, G. A. *Chem. Rev.* **2007**, *107*, 1272−1295.

(4) Beaujuge, P. M.; Fréchet, J. M. J. *J. Am. Chem. Soc.* **2011**, *133*, 20009−20029.

(5) Venkateshvaran, D.; Nikolka, M.; Sadhanala, A.; Lemaur, V.; Zelazny, M.; Kepa, M.; Hurhangee, M.; Kronemeijer, A. J.; Pecunia, V.; Nasrallah, I.; Romanov, I.; Broch, K.; McCulloch, I.; Emin, D.; Olivier,

DOI: 10.1021/acs.macromol.5b00707
Macromolecules XXXX, XXX, XXX−XXX

Y.; Cornil, J.; Beljonne, D.; Sirringhaus, H. *Nature* **2014**, *515*, 384−388.
(6) Beaujuge, P. M.; Reynolds, J. R. *Chem. Rev.* **2010**, *110*, 268−320.
(7) Wu, C.; Szymanski, C.; Cain, Z.; McNeill, J. *J. Am. Chem. Soc.* **2007**, *129*, 12904−12905.
(8) Kuehne, A. J. C.; Gather, M. C.; Sprakel, J. *Nat. Commun.* **2012**, *3*, 1088/1−7.
(9) Feng, L.; Zhu, C.; Yuan, H.; Lin, L.; Lv, F.; Wang, S. *Chem. Soc. Rev.* **2013**, *42*, 6620−6633.
(10) Kietzke, T.; Neher, D.; Landfester, K.; Montenegro, R.; Güntner, R.; Scherf, U. *Nat. Mater.* **2003**, *2*, 408−412.
(11) Hittinger, E.; Kokil, A.; Weder, C. *Angew. Chem., Int. Ed.* **2004**, *43*, 1808−1811.
(12) Yabu, H.; Tajima, A.; Higuchi, T.; Shimomura, M. *Chem. Commun.* **2008**, 4588−4589.
(13) Baier, M. C.; Huber, J.; Meching, S. *J. Am. Chem. Soc.* **2009**, *131*, 14267−14273.
(14) Pecher, J.; Mecking, S. *Chem. Rev.* **2010**, *110*, 6260−6279.
(15) Anwar, N.; Willms, T.; Grimme, B.; Kuehne, A. J. C. *ACS Macro Lett.* **2013**, *2*, 766−769.
(16) Xiao, X.; Bai, W.; Cai, L.; Lin, J. *Chem. Lett.* **2014**, *43*, 331−333.
(17) Adachi, T.; Tong, L.; Kuwabara, J.; Kanbara, T.; Saeki, A.; Seki, S.; Yamamoto, Y. *J. Am. Chem. Soc.* **2013**, *135*, 870−876.
(18) Tong, L.; Kushida, S.; Kuwabara, J.; Kanbara, T.; Ishii, N.; Saeki, A.; Seki, S.; Furumi, S.; Yamamoto, Y. *Polym. Chem.* **2014**, *5*, 3583−3587.
(19) Tabata, K.; Braam, D.; Kushida, S.; Tong, L.; Kuwabara, J.; Kanbara, T.; Beckel, A.; Lorke, A.; Yamamoto, Y. *Sci. Rep.* **2014**, *4*, 5902/1−5.
(20) Fichou, D.; Delysse, S.; Nunzi, J.-M. *Adv. Mater.* **1997**, *9*, 1178−1181.
(21) Zhu, X.; Gindre, D.; Mercier, N.; Frene, P.; Nunzi, J.-M. *Adv. Mater.* **2003**, *15*, 906−909.
(22) Ichikawa, M.; Hibino, R.; Inoue, M.; Haritani, T.; Hotta, S.; Araki, K.; Koyama, T.; Taniguchi, Y. *Adv. Mater.* **2005**, *17*, 2073−2077.
(23) Ichikawa, M.; Nakamura, K.; Inoue, M.; Mishima, H.; Haritani, T.; Hibino, R.; Koyama, T.; Taniguchi, Y. *Appl. Phys. Lett.* **2005**, *87*, 211113.
(24) Shimizu, K.; Mori, Y.; Hotta, S. *J. Appl. Phys.* **2006**, *99*, 063505.
(25) Frolov, S. V.; Shkunov, M.; Vardeny, Z. V.; Yoshino, K. *Phys. Rev. B* **1997**, *56*, R4363−R4366.
(26) Kawabe, Y.; Spiegelberg, Ch.; Schülzgen, A.; Nabor, M. F.; Kippelen, B.; Mash, E. A.; Allemand, P. M.; Kuwata-Gonokami, M.; Takeda, K.; Peyghambarian, N. *Appl. Phys. Lett.* **1998**, *72*, 141−143.
(27) Oraevsky, A. N. *Quantum Electron.* **2002**, *32*, 377−400.
(28) Vahala, K. J. *Nature* **2003**, *424*, 839−846.
(29) Matsko, A. B.; Savchenkov, A. A.; Strekalov, D.; Ilchenko, V. S.; Maleki, L. *IPN Prog. Rep.* **2005**, *42−162*, 1−51.
(30) Ta, V. D.; Chen, R.; Sun, H. D. *Sci. Rep.* **2013**, *3*, 1362/1−5.
(31) Ta, V. D.; Chen, R.; Ma, L.; Ying, Y. J.; Sun, H. D. *Laser Photonics Rev.* **2013**, *7*, 133−139.
(32) Kukino, M.; Kuwabara, J.; Matsuishi, K.; Fukuda, T.; Kanbara, T. *Chem. Lett.* **2010**, *39*, 1248−1250.
(33) Fujinami, Y.; Kuwabara, J.; Lu, W.; Hayashi, H.; Kanbara, T. *ACS Macro Lett.* **2012**, *1*, 67−70.
(34) Taniguchi, M.; Nojima, Y.; Yokota, K.; Terao, J.; Sato, K.; Kambe, N.; Kawai, T. *J. Am. Chem. Soc.* **2006**, *128*, 15062−15063.
(35) Frampton, M. J.; Anderson, H. L. *Angew. Chem., Int. Ed.* **2007**, *46*, 1028.
(36) Swager, T. M. *Acc. Chem. Res.* **2008**, *41*, 1181−1189.
(37) Sugiyasu, K.; Honsho, Y.; Harrison, R. M.; Sato, A.; Yasuda, T.; Seki, S.; Takeuchi, M. *J. Am. Chem. Soc.* **2010**, *132*, 14754−14756.
(38) Pan, C.; Sugiyasu, K.; Wakayama, Y.; Sato, A.; Takeuchi, M. *Angew. Chem., Int. Ed.* **2013**, *52*, 10775−10779.
(39) Terao, J.; Wadahama, A.; Matono, A.; Tada, T.; Watanabe, S.; Seki, S.; Fujihara, T.; Tsuji, Y. *Nat. Commun.* **2013**, *4*, 1691/1−9.
(40) Pan, C.; Sugiyasu, K.; Takeuchi, M. *Chem. Commun.* **2014**, *50*, 11814−11817.
(41) Braam, D.; Mölleken, A.; Prinz, G. M.; Notthoff, C.; Geller, M.; Lorke, A. *Phys. Rev. B* **2013**, *88*, 125302.
(42) McColloch, B.; Ho, V.; Hoarfrost, M.; Stanley, C.; Do, C.; Heller, W. T.; Segalman, R. A. *Macromolecules* **2013**, *46*, 1899−1907.
(43) Wei, C.; Liu, S.-Y.; Zou, C.-L.; Liu, Y.; Yao, J.; Zhao, Y. S. *J. Am. Chem. Soc.* **2015**, *137*, 62−65.

DOI: 10.1021/acs.macromol.5b00707
Macromolecules XXXX, XXX, XXX−XXX